Sensors and Materials, Vol. 36, No. 4 (2024) 1329–1336
MYU Tokyo

S & M 3601

Fiber-tip-integrated High-sensitivity Refractive Index and High-precision Liquid Level Sensor Based on Surface Plasmon Resonance

Guibin Yuan,[1] Shufei Han,[1] Min Yuan,[1] Xinjun Huang,[1] and Shengli Pu,[1,2*]

[1]University of Shanghai for Science and Technology, Shanghai 200093, China
[2]Shanghai Key Laboratory of Modern Optical System, University of Shanghai for Science and Technology, Shanghai 200093, China

(Received December 28, 2023; accepted February 28, 2024)

Keywords: surface plasmon resonance, refractive index sensor, liquid level sensor, multimode-no-core fiber tip

A refractive index (RI) and liquid level sensing scheme based on a multimode-no-core fiber tip with high sensitivity and precision is proposed and experimentally demonstrated by fusing a tapered no-core fiber (NCF) with a segment of multimode fiber. A gold film is plated on the side surface of the uniform waist region of the tapered NCF to stimulate surface plasmon resonance. The as-fabricated sensor achieves RI sensitivities of 16500 and 24000 nm/RIU (refractive index unit) in the RI ranges of 1.34 to 1.38 and 1.39 to 1.41, respectively. High-precision liquid level sensing with a range from 0.1 to 2.0 mm is obtained simultaneously. The designed sensing structure in this work offers simplicity and ease of implementation, which makes it a promising option for high-sensitivity and high-precision sensing applications.

1. Introduction

Refractive index (RI) is the basic physical property of a substance, and RI sensing can be used in various processes such as in biomedicine, pH detection, food processing, and chemical reaction.[1–3] Optical fiber sensing for RI measurement has been widely implemented because of its advantages of anti-electromagnetic interference, strong remote monitoring ability, and low price.[4–7]

Similarly, high-precision liquid level sensing is of considerable significance in chemical industry, oil storage, public water supply, and so forth. By monitoring the changes in physical quantities related to liquid level information, the remote monitoring and control of liquid level can be achieved. Since optical fibers have advantages of anti-electromagnetism and anti-high temperature, and are appropriate for application in flammable and explosive scenes, the optical fiber liquid level sensor has been widely used.[8–10]

At present, there are two types of optical fiber liquid level sensor: fiber grating sensor[11–13] and fiber mode interference sensor.[14–16] In 2018, Consales *et al.* proposed a fiber Bragg grating

*Corresponding author: e-mail: shlpu@usst.edu.cn
https://doi.org/10.18494/SAM4832

ISSN 0914-4935 © MYU K.K.
https://myukk.org/

(FBG) liquid level sensor with a sensitivity of ~27 pm/cm.[11] Compared with the grating sensor mentioned above, the mode-interference-type liquid level sensors made with biconical fiber, D-type fiber, dislocation fiber, and other fibers have relatively high sensitivity. For example, Tian *et al.* proposed a liquid level sensor based on an asymmetric dual side-hole fiber with a high pure water sensitivity of 4.019 nm/mm in 2019.[16] However, the mode-interference-type sensors usually have the disadvantage of relatively poor structural robustness.

Most optical fiber sensors based on the SPR effect need to remove the fiber cladding by chemical corrosion, side-polishing, tapering, and so forth. Then, the evanescent wave of the optical fiber can excite the surface plasma wave at the metal-external environment interface. The no-core fiber (NCF) as a special optical fiber has unique transmission characteristics.[17] When light is transmitted in the NCF, the NCF can be considered as the core and the external environment can be considered as the cladding. Therefore, evanescent waves can be generated at the interface of the optical fiber and the external environment. When the evanescent wave phase-matches with the plasma wave on the metal surface, the SPR effect occurs. By appropriately controlling the core diameter of the NCF, a high-quality output spectrum can be obtained.[18]

In this work, a reflective probe of multimode (MMF)-NCF structure is designed by splicing an MMF with a tapered NCF. The NCF end is cut off from the waist area to form an MMF-NCF tip, and then the uniform waist area of the fiber tip and the tip surface is gold-plated to achieve high-sensitivity RI sensing and high-precision liquid level sensing.

2. Fabrication and Sensing Principle

Figure 1(a) shows the schematic structure of the proposed RI and liquid level sensor in this work. The fabrication processes used are as follows. First, an MMF (diameters of the fiber core and cladding are 105 and 125 μm, respectively) is fused with an NCF (diameter of the cladding is 125 μm) of about 3 cm length using a fusion splicer (Fujikura 80C+), and then the fused fiber is tapered into a microfiber with a uniform waist area diameter of about 72 μm using a tapering machine (Shanghai Oubo Optoelectronics Technology Co., Ltd.). Then, the NCF is cut from the

(a)

(b)

Fig. 1. (Color online) (a) Schematic structure of the refractive index and liquid level sensor. (b) Microscopy image of the as-fabricated sensor.

uniform waist area to make the multi-mode NCF tip (MMF-NCF-tip). The finally obtained sensor is shown in Fig. 1(b).

The MMF-NCF-tip structure is inserted into an optical fiber connector with an aperture of 125 μm and the length of the exposed uniform NCF tip is 2 mm. Then, we put the NCF tip into the magnetron sputtering instrument (ETD-900M, Elaborate Technology Development Ltd. Co., China) vertically, about 2 cm away from the gold target, and coat the end face and the side surface of the exposed uniform area with gold film. The coating time is set to 180 ms. After the coating is finished, we take out the sample from the magnetron sputtering instrument and take out the joint along the other end of the fiber tip to avoid damaging the plated gold film. The gold film at the end of the optical fiber mainly plays a reflection role, and the gold film on the side surface of the optical fiber is used to stimulate SPR.

Since the diameter of the NCF is relatively larger than the wavelength of the incident light, the ray optics method is used to describe the transmission of light in the optical NCF tip, as shown in Fig. 2.

After the light is reflected through the gradient region many times, it is coupled into the uniform tip region at an incident angle θ_n, and the evanescent field generated in the uniform tip region will be coupled to the surrounding medium. When the wave vector k_{spp} of the polariton generated at the interface and the evanescent wave vector k_{0x} coupled to the surrounding medium are equal, phase matching occurs.[19] Then, plasmon resonance occurs on the surface of the gold film, i.e.,

$$k_{0x} = k_{spp}\,, \tag{1}$$

$$k_{0x} = \frac{\omega}{c}\sqrt{\varepsilon_f}\sin\theta_n\,, \tag{2}$$

$$k_{spp} = \frac{\omega}{c}\sqrt{\frac{\varepsilon_1 \cdot \varepsilon_2}{\varepsilon_1 + \varepsilon_2}}\,, \tag{3}$$

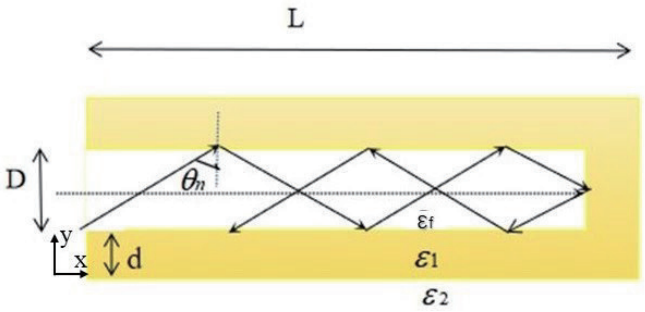

Fig. 2. (Color online) Propagation of light in the NCF sensing area.

where ω is the frequency of the light wave, c is the propagation rate of light in vacuum, and ε_f, ε_1, and ε_2 are the dielectric constants of the optical fiber, gold film, and external environment media, respectively.

When the light is transmitted to the end face of the NCF tip, it will be retroreflected through the reflector formed by the gold film on the end face. Thus, the sensing length of the reflective probe of the fiber tip structure is twice the actual length of the sensing fiber. Whenever SPR occurs in the fiber tip, the energy of the incident light will be lost once; thus, the total reflection coefficient is the accumulation of each reflection coefficient. Suppose that the number of total reflections at the optical fiber tip is

$$N(L, D, \theta_n) = \frac{L}{D \tan \theta_n}, \tag{4}$$

where L is the sensing length of the NCF tip coated with gold film and D is the diameter of the NCF tip.

The total reflection coefficient of the optical fiber tip reflection probe can be expressed as a complex function of multiple parameters:[20]

$$R = r\left[\theta_n, d, L, n_m(\lambda, d), n_f(\lambda), n_s(\lambda)\right]^{N(L,D,\theta_n)}, \tag{5}$$

where the reflection coefficient r of the primary reflection is related to the thickness d of the gold film, the complex refractive index n_m of the gold film, the refractive index n_f of the optical fiber, and the refractive index n_s of the environmental medium.

It can be seen from Eq. (5) that the reflection spectrum is closely related to the n_s of the ambient medium. Next, we will discuss the sensing properties of the SPR-based tapered NCF tip at different external RIs and liquid levels.

3. Experiment Details and Discussion

The experimental setup for measuring the RI and liquid level is shown in Fig. 3. The sensing system includes a halogen light source [360–2000 nm, HL - 2000, Ocean Optics (Shanghai) Co., Ltd., China], a Y-type coupler, the sensing structure, a spectrometer [USB 4000, Ocean Optics (Shanghai) Co., Ltd., China], and a computer. The sensing device is fixed on the micro-controllable lift platform to facilitate the precise control and adjustment of the immersion depth of the MMF-NCF-tip structure into the liquid. During the experiment, the reflectance spectrum was collected by the spectrometer and recorded and analyzed by the computer.

For the first experiments, an MMF-NCF-tip structure with a 72-μm-wide NCF-tip waist area is fabricated. The length of the gold-film-coated area is 2 mm. Its SPR valley in water is shown in Fig. 4. For comparison, Fig. 4 also shows the MMF-NCF-tip reflectance spectrum with an NCF-tip width of 125 μm (i.e., untapered NCF). Figure 4 shows that the SPR valley generated by the tapered NCF tip with a diameter of 72 μm is deeper than that of the untapered NCF tip with

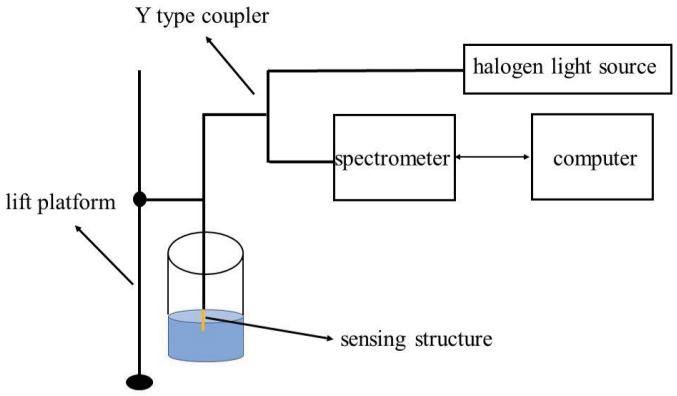

Fig. 3. (Color online) SPR sensing system with MMF-NCF-tip structure.

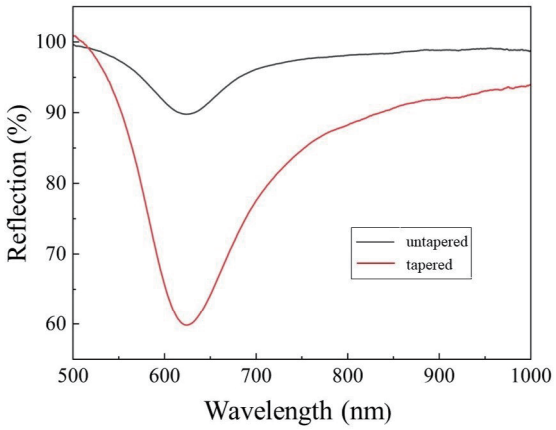

Fig. 4. (Color online) SPR valleys corresponding to tapered and untapered NCF tips.

a diameter of 125 μm, making the spectrum easier to identify. This is because when light is transmitted into the conical region, the reflection angle of the forward transmitted light becomes increasingly smaller, which gradually approaches the critical angle of the total reflection in the NCF, and then the penetration depth increases and improves the transmission effect of the evanescent wave into the sensing medium, thereby maximizing the coupling between the evanescent wave and the surface plasma wave. Therefore, a small taper with good spectral performance is the best choice. In the following, an NCF tip with a waist diameter of 72 μm is used as the sensor sample to investigate the sensing performance under different RI liquid environments and liquid level heights. All the experiments are conducted at constant room temperature (25 °C).

Before the RI sensing experiment, we prepared a group of glycerol solutions of different concentrations, corresponding to the RI in the range of 1.33–1.41 measured using the Abbe refractometer, with an interval of 0.01. When the NCF tip is immersed in different glycerol solutions but with the same depth (0.5 mm), the measured reflection spectrum is as shown in Fig.

5(a). Figure 5(a) shows that as the RI of the glycerol solution increases, the SPR resonance wavelength shifts toward the long wavelength direction. As described in Eq. (5), the total reflection coefficient is related to the RI of the glycerol solution. Thus, the SPR resonance wavelength drifts with the ambient RI, and the experimental results are in agreement with the theoretical predictions.

By monitoring the position of the resonance wavelength under different RIs, the relationship between the resonance wavelength and RI is obtained and shown in Fig. 5(b). The results show that in the RI ranges from 1.34 to 1.38 and 1.39 to 1.41, the sensitivities are 16500 and 24000 nm/RIU, respectively. Comparatively, the sensitivity of the previously proposed RI sensor is generally on the order of 10^3.[21,22] Therefore, the structure of the MMF-NCF tip in this study realizes the RI sensing with ultrahigh sensitivity.

During the liquid level sensing experiment, the MMF-NCF-tip sensing structure is immersed in water with an adjustable immersion depth. Figure 6(a) shows the SPR spectral curves measured in the range of 0–2 mm. Figure 6(a) shows that with the increase in liquid level depth, the reflection intensity of the SPR resonance valley becomes increasingly smaller, which is manifested as the depth of the valley becomes increasingly deeper, while the resonance wavelength hardly changes. The reason is that the evanescent wave generated by the total reflection of the NCF tip cannot be effectively coupled to a small surrounding medium such as air (corresponding to the unimmersed part) to excite the SPR, but it can be achieved if the surrounding environment is water (a high-refractive-index medium, corresponding to the immersed part).[23] Therefore, as the depth of immersion gradually increases, more energy is lost owing to the cumulative attenuated total reflection, and then the resonance valley becomes deeper. By monitoring the depth of the valley at different liquid levels, the variation relationship between the valley depth and the liquid level is obtained and shown in Fig. 6(b). Figure 6(b) shows that for the first 1 mm variation range of the liquid level, the depth of the valley changes considerably, while for the second 1 mm variation range of the liquid level, the depth of the valley changes relatively little. The possible reason is that the surface tension of the water makes

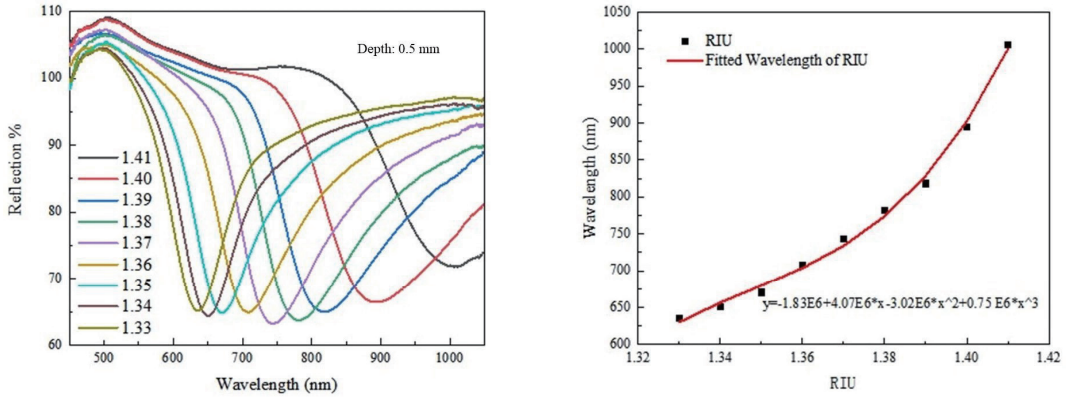

(a) (b)

Fig. 5. (Color online) (a) SPR valleys under different RIs and (b) relationship between the wavelength of SPR valley and RI.

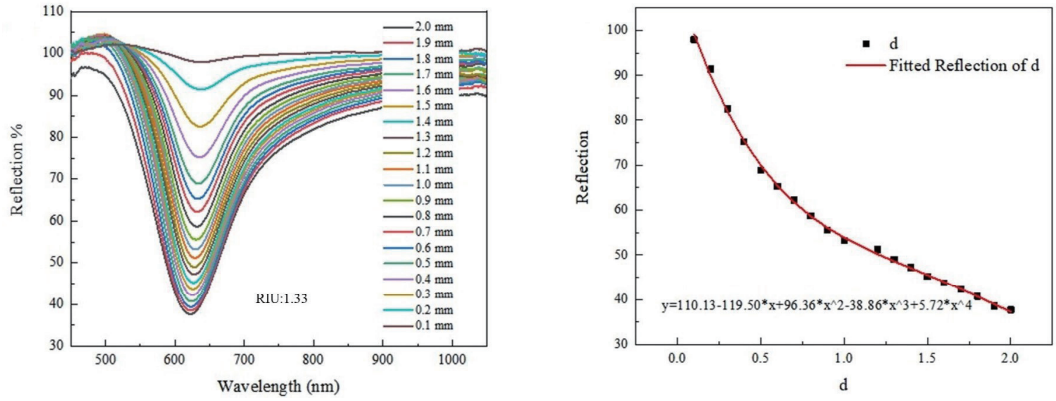

(a) (b)

Fig. 6. (Color online) (a) SPR valleys at different liquid levels and (b) relationship between the depth of SPR valley and the change in liquid level.

the actual height of the water larger than the height measured in the experiment; that is, within the range of the measured liquid level of 1–2 mm, the actual liquid level is higher than the sensing length of the entire coating. The sensor structure achieves a level monitoring accuracy of 0.1 mm, and a higher measurement accuracy can be achieved according to actual needs. Compared with previous liquid level sensing results, such as the 0.26 mm monitoring accuracy achieved by Dong *et al.*'s D-type optical fiber liquid level sensor based on the principle of mode interference[14] and the 0.4 mm monitoring accuracy achieved by Consales *et al.*'s fiber Bragg grating liquid level sensor based on Archimedes' buoyancy law,[11] this sensing structure achieves a higher precision liquid level sensing.

It should be pointed out that the designed sensor realizes RI and liquid level sensing based on two separate interrogation mechanisms, namely, wavelength interrogation and intensity interrogation, respectively. Therefore, it can intrinsically solve the cross-sensitivity problem through a single integrated sensor with a compact footprint.

4. Conclusions

In this work, an MMF-NCF-tip structure based on the SPR effect is proposed to realize high-sensitivity RI sensing and high-precision liquid level sensing. The effect of a small taper on the SPR of the optical fiber tip and the mechanism of SPR spectra under different RIs and liquid levels are analyzed. By monitoring the SPR valley of the NCF tip with a small taper, the RI sensing with a sensitivity of 24000 nm/RIU and the liquid level sensing with a high precision of 0.1 mm are obtained experimentally. The sensor structure designed in this work has advantages of simple and easy implementation, intrinsic immunity to cross-sensitivity, and high integration and miniaturization, and has broad prospects in the application of high-sensitivity and high-precision sensing.

Acknowledgments

This work was jointly supported by the National Natural Science Foundation of China (Grant No. 62075130), the Natural Science Foundation of Shanghai (Grant No. 23ZR1443300), and the Program of Shanghai Academic Research Leader (Grant No. 23XD1402200).

References

1 K. Yatim, G. Krishnan, H. Bakhtiar, S. Daud, and S. Harun: J. Phys. Conf. Ser. **1371** (2019) 012021. https://doi.org/10.1088/1742-6596/1371/1/012021
2 R. Zhao, T. Lang, J. Chen, and J. Hu: Opt. Eng. **56** (2017) 1. https://doi.org/10.1117/1.OE.56.5.057113
3 W. Luo, B. Liu, J. Liu, T. Wu, Q. Liu, M. Wang, S. Wan, J. Yuan, P. Lu, D. Wang, X. He, and Q. Wu: IEEE Sens. J. **22** (2022) 7727. https://doi.org/10.1109/JSEN.2022.3156284
4 Z. Yin and X. Jing: IEEE Trans. Instrum. Meas. **72** (2023) 1. https://doi.org/10.1109/TIM.2023.3324676
5 P. Wang, J. Hu, C. Jiang, L. Deng, C. Hu, J. Gao, L. Li, and H. Li: Optik **289** (2023) 171289. https://doi.org/10.1016/j.ijleo.2023.171289
6 J. Wang, G. Sun, Y. Ning, Z. Li, L. Zhao, J. Wang, T. Liu, W. Zhang, G. Dong, and K. Grattan: Meas. Sci. Technol. **34** (2023) 055114. http://doi.org/10.1088/1361-6501/acbab5
7 H. Fu, C. Liu, L. Xu, W. Liu, J. Lv, J. Wang, J. He, X. Luo, and P. Chu: J. Opt. Soc. Am. A: **40** (2023) 2177. https://doi.org/10.1364/JOSAA.499894
8 J. Shi, Z. Xu, X. Li, H. Bai, C. Guo, P. Niu, and J. Yao: IEEE Sens. J. **23** (2023) 16938. https://doi.org/10.1109/JSEN.2023.3288223
9 Q. Liu, T. Liu, T. He, H. Li, Z. Yan, L. Zhang, and Q. Sun: Opt. Express. **29** (2021) 11538. https://doi.org/10.1364/OE.412935
10 E. Dejband, Y. Manie, Y. Deng, M. Bitew, T. Tan, and P. Peng: Sensors **23** (2023) 1. https://doi.org/10.3390/s23042360
11 M. Consales, S. Principe, A. Iele, M. Leone, H. Zaraket, I. Jomaa, A. Cutolo, and A. Cusano: J. Lightwave Technol. **36** (2018) 4936. https://doi.org/10.1109/JLT.2018.2866130
12 D. Song, J. Zou, Z. Wei, Z. Chen, and H. Cui: Opt. Eng. **50** (2011) 014401. https://doi.org/10.1117/1.3525286
13 B. Yun, N. Chen, and Y. Cui: IEEE Photonics Technol. Lett. **19** (2007) 1747. https://doi.org/10.1109/LPT.2007.905093
14 Y. Dong, S. Xiao, H. Xiao, J. Liu, C. Sun, and S. Jian: IEEE Photonics Technol. Lett. **29** (2017) 1067. https://doi.org/10.1109/LPT.2017.2700623
15 M. Sun, Y. Jin, and X. Dong: IEEE Sens. J. **15** (2015) 3984. https://doi.org/10.1109/JSEN.2015.2406872
16 Y. Tian, T. Tan, C. Duan, B. Xu, X. Zhao, Q. Chai, J. Ren, J. Zhang, E. Lewis, Y. Liu, J. Yang, and L. Yuan: Opt. Commun. **440** (2019) 194. https://doi.org/10.1016/j.optcom.2019.02.019
17 S. Bi, C. Wang, J. Zhu, Z. Yuan, Y. Yu, S. Valyukh, and A. Asundi: Opt. Lasers Eng. **107** (2018) 46. https://doi.org/10.1016/j.optlaseng.2018.03.008
18 Z. Ding, T. Lang, Y. Wang, and C. Zhao: J. Lightwave Technol. **35** (2017) 4734. https://doi.org/10.1109/JLT.2017.2755668
19 Y. Zhao, M. Lei, S. Liu, and Q. Zhao: Sens. Actuators, B **261** (2018) 226. https://doi.org/10.1016/j.snb.2018.01.120
20 A. Scheggi, M. Niggemann, A. Katerkamp, P. Bolsmann, J. Reinbold, and K. Cammann: Proc. SPIE - The International Society for Optical Engineering **2508** (1995) 303. https://doi.org/10.1117/12.221744
21 H. Hu, X. Song, Q. Han, P. Chang, J. Zhang, K. Liu, Y. Du, H. Wang, and T. Liu: IEEE Sens. J. **20** (2020) 2967. https://doi.org/10.1109/JSEN.2019.2956559
22 Y. Wang, S. Li, Y. Guo, S. Zhang, and H. Li: Infrared Phys. Technol. **114** (2021) 103685. https://doi.org/10.1016/j.infrared.2021.103685
23 C. Caucheteur, T. Guo, F. Liu, B. Guan, and J. Albert: Nat. Commun. **7** (2016) 1. https://doi.org/10.1038/ncomms13371